RSC Advances

Accepted Manuscript

This article can be cited before page numbers have been issued, to do this please use: C. Ye, C. Guo, C. Sun and Y. Zhang, *RSC Adv.*, 2016, DOI: 10.1039/C6RA24252A.

ROYAL SOCIETY OF CHEMISTRY

rsc.li/rsc-advances

View Article Online
DOI: 10.1039/C6RA24252A

Effect of Mn doping on the activity and stability of Cu-SiO_2 catalysts for the hydrogenation of methyl acetate to ethanol

Chenliang Ye, Cuili Guo*, Chenwei Sun, Yu Zhang

School of Chemical Engineering and Technology, Tianjin University, Tianjin 300072, China

ABSTRACT

A series of xMn-Cu-SiO_2 catalysts with different manganese contents were prepared by an ammonia-evaporation method for methyl acetate hydrogenation. The activity and stability of the catalysts were greatly improved when manganese content was 3%. Besides, physicochemical properties of these catalysts were investigated by N_2 physisorption, X-ray diffraction, H_2-temperature programmed reduction and X-ray photoelectron spectroscopy. The results illustrated that doping a suitable amount of manganese to silica-supported copper catalysts produced a strong interaction between cupreous species and Mn, diminished the copper crystalline size，enlarged the copper surface area and enriched the surface Cu^+ species, so as to improve the catalytic activity and stability of the 3Mn-Cu-SiO_2 catalyst.

Keywords: Methyl acetate; Hydrogenation; Manganese; Cu-SiO_2 catalyst

1. Introduction

Ethanol, one of the most important basic materials, plays an important role in fuel additive, chemical feedstock, medical treatment, and so on [1]. In particular, the mixture of ethanol and petrol can prepare ethanol-petrol fuels, the use of which will slow down the depletion of oil resources and reduce the pollution of air [2]. Nowadays, ethanol is mainly synthesized from ethylene hydration and microbial fermentation of biomass [3]. However, due to the shrinking oil resource and costly biological process, the established methods have faced many challenges [1]. Thus, it

Corresponding author: Cuili Guo, School of Chemical Engineering & Technology, Tianjin University, Tianjin, 300072; Tel: +86-22-2270-4495; E-mail: gcl@tju.edu.cn

View Article Online
DOI: 10.1039/C6RA24252A

is of critical significance to explore new methods to meet increasing demands of ethanol. Nowadays, methyl acetate (MA) is mainly resulted from natural gas and coal [4, 5]. Because of the recent surge in shale gas production and the large amount of coal reserve in the world, hydrogenation of methyl acetate become a very economic process to synthesis ethanol.

Hydrogenation of MA to synthesis ethanol can be described as following:

$$CH_3COOCH_3+H_2 \rightarrow CH_3CH_2OH+CH_3OH \quad (1)$$

Besides, transesterification, the main side reaction, often occurs during the process[6].

$$CH_3COOCH_3+ CH_3CH_2OH \rightarrow CH_3COOCH_2CH_3+CH_3OH \quad (2)$$

For ester hydrogenation, the traditional catalysts are chromium oxide supported copper-based catalysts [7, 8]. Although the chromium-supported copper catalysts achieve quite good activity and stability, the use of chromium makes a severe pollution to the environments. Hence, the research of chromium-free catalysts is of great importance. To develop chromium-free catalysts, most of studies have been focused on Cu-SiO_2 catalysts, because a high initial copper surface area on silica supports was believed to obtain good catalytic performance for ester hydrogenation [9]. The main researches on Cu-SiO_2 catalysts are preparation methods and promoter additives. The research on preparation methods, such as ammonia evaporation, deposition precipitation, impregnation and ion exchange method, indicated that different preparation methods made a great influence on the metal-support interaction [10-13]. The studies in promoter additives of Cu-SiO_2 catalysts showed that additives, such as Zn, Mo, Ni, B and Mg, can dramatically change the catalytic performance of Cu-SiO_2 catalysts [6, 9, 14-17]. However, there are still many challenges of silica-supported copper catalysts need to be overcome, especially the inherent insufficient lifespan.

In methanol synthesis and dimethyl ether synthesis from syngas, it has been suggested that the interaction between copper and manganese could greatly change the chemical states of cupreous species [18, 19]. In addition, in CO hydrogenation reaction, it also has been reported that Manganese was an effective promoter for

View Article Online
DOI: 10.1039/C6RA24252A

ethanol synthesis [20]. However, a detailed research related to the influence of Mn doping on Cu-SiO_2 catalysts for MA hydrogenation has not been reported. In this paper, a series of Mn-modified Cu-SiO_2 catalysts with different manganese doping amount were prepared by an ammonia-evaporation method, and their catalytic performances for hydrogenation of MA were evaluated in a fixed-bed reactor. Besides, several characterizations were carried out to investigate the relationship between the structure and catalytic performance of the catalysts. The main aim of this study is to develop catalysts with enhanced catalytic activity and lifespan for MA hydrogenation.

2. Experimental

2.1. Catalyst preparation

A series of xMn-Cu-SiO_2 catalysts with copper content of 30% were synthetized by an ammonia-evaporation method, where x is the mass loading of Mn. With a typical procedure, a certain amount of $Mn(NO_3)_2{\cdot}4H_2O$ and $Cu(NO_3)_2.3H_2O$ were dissolved in 100 mL deionized water under stirring. An appropriate amount of 25 % ammonia aqueous solution was added and stirred for 0.5 h. The initial pH of the suspension was 11-12. Next, a certain amount of 25 % silica sol was added to the above suspension and stirred for 3 h. All the operations mentioned above were conducted at room temperature. Then, the suspension was heated at 363 K in a water bath to evaporate the ammonias. When the pH value of the suspension decreased to 6-7, the evaporation process was completed. Finally, the precipitate was dried at 393 K for 24 h and calcined at 723 K for 4 h to get the catalyst precursor. For comparison, the Mn-SiO_2 catalyst with manganese loading of 3% was also prepared by the same method as above.

2.2. Catalytic Activity Tests

The activity of the catalysts was tested in a fixed-bed tubular reactor with an internal diameter of 10 mm. A certain amount of catalysts were activated by pure hydrogen (250 mL/min) at 623 K for 4 h, with a heating rate of 5 K/min starting from room temperature. After cooling to the reaction temperature, MA was injected to a gasification chamber by a high-pressure pump and mixed with hydrogen. Then, the mixture went into the reactor and started reaction. The products were condensed and

View Article Online
DOI: 10.1039/C6RA24252A

analyzed by a gas chromatograph (North Branch of Ruili SP-3200A) fitted with a HJ-WAX capillary column and a flame ionization detector (FID).

The conversion and selectivity of products were calculated based on the following equations：

$$\text{Conversion}(\%) = 100 - \frac{\text{Amount of MA after reaction(mol)}}{\text{Total amount of MA in the feed(mol)}} \times 100 \quad (3)$$

$$\text{Selectivity}(\%) = \frac{\text{Amount of ethanol(mol)}}{\text{Total amount of MA converted(mol)}} \times 100 \quad (4)$$

2.3. Catalyst characterization

The textual properties of the catalysts were measured by the method of N_2 physisorption using a Quantachrome Nova 2200e instrument. Before the analysis, the catalysts were outgassed at 573 K for 3 h under vacuum. The specific surface areas were figured out by the Brunauer-Emmett-Teller (BET) equation and the total pore volume (V_p) was calculated d from the adsorbed N_2 volume at a relative pressure of approximately 0.99.

H_2 temperature programmed reduction (TPR) was conducted by a Quantachrome Instrument AMI-90. Before the reduction, 100 mg catalyst was under He flow (30 mL/min) at 373 K for 0.5 h to drive off physically adsorbed impurities. Then the catalyst was reduced by 10 vol.% H_2/Ar (30mL/min) from 373 K to 1073 K with a heating rate of 10 K/min. The consumption of hydrogen was tested by a thermal conductivity detector (TCD).

The X-ray diffraction (XRD) was executed on a D/MAX-2500 diffractometer using Cu Kα as the radiation source. The scanned range was from 30° to 90° with a scanning rate of 5°/min. The particle size of copper was estimated by Scherrer equation.

The Cu surface area was tested by N_2O chemisorption on a Quantachrome Instrument AMI-90，using a procedure described in the literatures [21, 22]. Firstly, 100 mg catalyst was reduced at 623 K for 4 h. Then, the N_2O pulse was conducted at 363 K, $Cu+N_2O \rightarrow Cu_2O+N_2$, and the consumption of N_2O was measured by a TCD detector. The Cu surface area was calculated from the total amount of N_2O consumption with 1.46×10^{19} copper atoms/m^2.

View Article Online
DOI: 10.1039/C6RA24252A

X-ray photoelectron spectroscopy (XPS) and X-ray induced Auger spectra (XAES) were performed on a PHI5000 VersaProbe spectrometer with monochromatic Al Kα (E=1486.6eV) as the excitation source. Adventitious carbon (C1s = 284.8 eV) was used to calibrate the binding energies.

3. Results

3.1. Catalytic performance of the catalysts

The influence of manganese content on the catalytic activity of xMn-Cu-SiO_2 catalysts for MA hydrogenation is shown in Table 1 (Reaction time was 8 h). The effect of external diffusion and internal diffusion was eliminated during the activity test (See the supporting information). The ethanol yield of 3Mn-SiO_2 catalyst was 0, which suggested that Mn-based catalysts without Cu do not show any catalytic activity for MA hydrogenation. For the Mn modified Cu-SiO_2 catalysts, both MA conversion and ethanol selectivity were gradually enhanced with the increasing amount of manganese loading and reached to a maximum when the manganese loading reached 3%. The 3Mn-Cu-SiO_2 catalyst achieved 96.2% MA conversion and 95.2% ethanol selectivity, which were considerably better than the results of the Cu-SiO_2 catalyst. However, further increase the amount of manganese loading resulted in a decrease in both MA conversion and ethanol selectivity. The 8Mn-Cu-SiO_2 catalyst obtained a very low ethanol yield, only 27.8%. These results suggested that adoption of a proper amount of manganese to Cu-SiO_2 catalysts was of critical importance to improve the catalytic activity for MA hydrogenation.

From both academic and industrial viewpoints, the stability of the catalysts is of great importance besides activity and selectivity. A comparison of catalytic activity as a function of reaction time on stream for the Cu-SiO_2 catalyst and the 3Mn-Cu-SiO_2 catalyst is showed in Fig.1. The 3Mn-Cu-SiO_2 catalyst maintained its high catalytic activity during the 100 h stability test. For the Cu-SiO_2 catalyst, the MA conversion and ethanol selectivity decreased to about 69% and 79% respectively after 100 h stability test. For ester hydrogenation, it has been widely acknowledged that the deactivation of copper-based catalysts mainly results from copper aggregation and the valence transition of cupreous species [9, 23].These results indicated that adding a

View Article Online
DOI: 10.1039/C6RA24252A

suitable amount of manganese to Cu-SiO_2 catalysts was an effective way to improve the stability of silica-supported copper catalysts.

3.2. Characterization of the catalysts

3.2.1. Physicochemical properties of the catalysts

The textural properties of different manganese content catalysts were investigated. As shown in Table 2, the Cu-SiO_2 catalyst had a relatively high BET surface area of 316 m^2/g. With the increase of manganese loading, the surface areas of the catalysts gradually decreased. When the manganese content reached 8%, the surface areas of the 8Mn-Cu-SiO_2 catalyst was very small, only 59 m^2/g. In contrast, the average pore size of the catalysts increased with the increase of manganese loading, and the average pore size reached 14.6 nm when the manganese content was 8%. It was noticeably that the average pore sizes of all the samples varied from 6.9-14.6 nm, which were typically mesoporous materials. The pore volume of the catalysts was also greatly affected by the content of manganese. When the manganese loading reached 3%, the largest pore volume was achieved. However, further increase of manganese loading, the pore volume of the catalysts declined sharply.

Copper surface area has been viewed as a crucial factor affecting catalytic performance of copper-based catalysts [24]. The copper surface area of the Cu-SiO_2 and the Mn-modified Cu-SiO_2 catalysts was determined by the N_2O chemisorption. As shown in Table 2, adding a suitable amount of manganese significantly enlarged the copper surface area. The highest copper surface area was acquired on the 3Mn-Cu-SiO_2 catalyst, which afforded the highest ethanol yield. Nevertheless, further increasing manganese content led to a decrease of copper surface area. These results indicated that adoption of a proper amount of manganese to Cu-SiO_2 catalysts was an effective way to enlarge the copper surface area.

3.2.2. Crystalline phase

To investigate the crystalline structure of the catalysts, the XRD of the calcined catalysts and reduced catalysts was carried out. As illustrated in Fig. 2 (A), the characteristic peaks positioned at 2θ of 35.5° and 38.7° correspond to (002) and (111) lattice planes of copper oxide species respectively [15]. With adoption of a small

View Article Online
DOI: 10.1039/C6RA24252A

amount of manganese to Cu-SiO_2 catalysts, the CuO diffraction peaks became wider and weak. However, too much manganese doping made CuO diffraction peaks become stronger and sharper. The 3Mn-Cu-SiO_2 catalyst exhibited the weakest CuO diffraction peaks, indicating that the copper species was better dispersed in the 3Mn-Cu-SiO_2 catalyst than other catalysts. Noticeably, no diffraction peaks attributed to manganic species were observed in all the catalysts, which might result from the low content of manages or well dispersion of manganic species.

The XRD patterns of the reduced catalysts were presented in Fig. 2(B). The characteristic peaks at 43.5°, 50.4° and 74.1° ascribed to the (111), (200) and (220) lattice planes of Cu^0 species were detected in all samples [15]. The peak intensities of Cu^0 species were firstly weakened and then strengthened with the increase of manganese loading. The 3Mn-Cu-SiO_2 catalyst had the weakest Cu^0 diffraction peak and the size of copper crystallite was the smallest, only 12.5 nm as shown in Table 2. Besides, a weak diffraction peak at 2θ of 36.6° ascribed to Cu_2O was observed for all the samples, and the 3Mn-Cu-SiO_2 catalyst also exhibited the weakest diffraction peak. It has been suggested that the active phase dispersion can be reflected by the peak intensity [9]. Thus, the 3Mn-Cu-SiO_2 catalyst achieved the best dispersion of active species among all the samples. These results suggested that adoption of a moderate amount of manganese to Cu-SiO_2 catalysts was an effective way to control the crystalline size of cupreous species and improve the copper dispersion (The TEM of the reduced catalysts can been seen in the supporting information).

3.2.3. Reducibility of the catalysts

To evaluate the reduction behaviour of the catalysts, the calcined Cu-SiO_2 and the Mn-modified Cu-SiO_2 catalysts were examined by H_2-TPR. As displayed in Fig. 3, the Cu-SiO_2 catalyst showed a unique reduction peak centered at 553 K, which might result from the collective effective of the reduction of Cu^{2+} to Cu^0 and Cu^{2+} to Cu^+ [25-27]. Obviously, adoption of manganese greatly affected reduction peak of the samples. The reduction peak of the samples gradually shifted to a higher temperature with the adoption of more manganese component, which indicated the strong chemical interaction between cupreous specious and manganese had occurred during

View Article Online
DOI: 10.1039/C6RA24252A

the reduction process [17, 19, 28, 29]. It has been suggested that the interaction between copper and Mn make CuO reduction more difficult and result in a higher reduction temperature of cupreous species [17]. This effect may account for smaller copper particles and higher stability of Mn-modified copper-based catalysts. For comparison, the reduction property of the 3Mn-SiO_2 catalyst was also carefully investigated. As shown in Fig.3, the 3Mn-SiO_2 catalyst showed two reduction peaks at 653 K and 798 K. It has been suggested that the two manganese reduction peaks correspond to the reduction of Mn^{4+} to lower oxidation states [17, 30]. Since the catalysts were reduced at 623 K for 3 h before activity test, the manganese valence of the reduced catalysts might coexist of different values.

3.2.4. Surface chemical states

Since manganese may be reduced during the reduction process, Mn 2p XPS was recorded to analyze the surface chemical state of reduced catalysts. It has been reported that Mn 2P XSP may display narrow peaks at 642.3 eV or 641.8 eV or 640.8 eV, corresponding to MnO_2, Mn_2O_3 and MnO [17, 31, 32]. As represented in Fig. 4, broad and asymmetric Auger peaks were observed in all the samples, suggesting significant overlap between different Mn species and Co-existence of multiple Mn valence state of all the reduced catalysts [17, 30]. These results are consistent with the TPR analysis.

To investigate the surface chemical states of copper species, the Cu 2P XPS patterns of reduced catalysts are shown in Fig. 5. Only two peaks around 952.6 eV and 932.8 eV were observed in the XPS, which were ascribed to Cu $2p_{1/2}$ and Cu $2p_{3/2}$ peaks, respectively. The disappearance of the 2p satellite peak centered at 942-944 eV indicated that all Cu^{2+} species had been reduced into Cu^0 or Cu^+ [12].

The binding energy is very close between Cu^0 and Cu^+. Thus, the Cu LMM XAES spectra was carried out to further distinguish the surface Cu^+ and Cu^0 species of reduced catalysts [33]. As Fig. 6 displays, the broad and asymmetric Auger peaks were observed, which indicated that Cu^0 and Cu^+ might coexist on the surfaces of the reduced catalysts. Besides, the coexistence of Cu^0 and Cu^+ species of the reduced catalysts was also proved in the XRD patterns. The Cu LMM XAES spectra could be

View Article Online
DOI: 10.1039/C6RA24252A

deconvoluted into two obvious overlapping peaks at 570.8 eV and 567.8 eV, which were ascribed to Cu^+ and Cu^0, respectively [33, 34]. The results of deconvolution were shown in Table 2. The distributions of surface Cu^+ and Cu^0 were greatly affected by the manganese loading. The mole ratio of $Cu^+/(Cu^0+Cu^+)$ firstly went up and then declined with the increase of manganese content. The maximum value of $Cu^+/(Cu^0+Cu^+)$ was 58.5% when the manganese loading reached 3%. Generally speaking, for copper-based catalysts, the distribution of copper valence is subjected to many factors, such as preparation method, type of silica species, copper loading, additives and so on .These results illustrated that adoption of manganese to Cu-SiO_2 catalysts was an effective way to control the distributions of surface Cu^+ and Cu^0.

4. Discussion

Although copper-based catalysts have been widely studied for acetic ester hydrogenation and various additives have been adopted to improve the catalytic performance of silica-supported copper catalysts, the insufficient activity and lifespan of silica-supported copper catalysts still remains a great challenge. Modifying with manganese was one of an effective way to improve catalytic performance of silica-supported copper catalysts, and the catalytic performance was strongly affected by the content of manganese loading. Compared to Cu-SiO_2 catalysts, the ethanol yield was increased from 77.3% to 91.6% when the loading of manganese reached 3%, and the 3Mn-Cu-SiO_2 catalyst exhibited quite better stability than the Cu-SiO_2 catalyst.

There was a strong correlation between the copper surface area and the ethanol yield. Among all the catalysts, the 3Mn-Cu-SiO_2 displayed the highest copper surface area, which afforded the highest ethanol yield. As XRD analysis illustrates, the 3Mn-Cu-SiO_2 catalyst achieved the smallest copper crystallite size. It has been suggested that smaller copper crystallite size tends to achieve higher copper dispersion and higher copper surface area, so as to improve the catalytic performance for ester hydrogenation [9, 35]. However, excessive adoption of manganese to Cu-SiO_2 catalysts led to an aggregation of copper and decrease the catalytic activity. As listed in table 2, adding manganese to Cu-SiO_2 resulted in a decrease of surface are

View Article Online
DOI: 10.1039/C6RA24252A

of the catalysts. When the amount of manganese loading reached 8%, the surface area of the catalyst was very small, only 42.7 m^2/g. Too small surface area might account for the aggregation of cupreous species and enlarge the copper crystalline size.

Although high reduction temperature is conducted to activated catalysts, the coexistence of Cu^+ and Cu^0 in silica-supported copper catalysts is generally accepted [9, 14, 34, 36, 37]. As well as the copper crystalline size, valence distribution of cupreous species is widely viewed as an important factor that affect catalytic performance of copper-based catalysts. In our Mn promoted copper-based catalysts, the ethanol yield and valence distribution of cupreous species were strongly changed by the amount of manganese loading. As shown in Table 1 and Table 2, the 3Mn-Cu-SiO_2 catalyst exhibited the highest ethanol yield and the largest mole ratio of $Cu^+/(Cu^0+ Cu^+)$. For ester hydrogenation, the cooperation of Cu^0 and Cu^+ for catalytic performance is widely accepted and it is of critical importance to obtain a balance valance distribution of Cu^0 and Cu^+ [9, 12, 25, 34]. It has been reported that the Cu^0 species dissociatively adsorbs H_2, and the Cu^+ species may stabilize the methoxy and the acyl specie [26]. Besides, Cu^+ sites may act as electrophilic or Lewis acid sites to polarize the C=O bond via the electron lone pair on oxygen [11, 29], which are beneficial for improving the activity of the ester groups. Thus, the improvement of catalytic activity of the Mn-modified copper-based catalysts could be partly attributed to the enrichment of surface Cu^+ species.

Adoption of manganese to copper-based catalysts strongly affected the chemical state of cupreous species, including copper crystalline size, valance distribution and reduction temperature. In Mn promoted copper-based catalysts, it has been suggested that Mn^{3+} species is of critical importance to the Mn promotion effect, since the appropriate oxidation ability of Mn^{3+} could oxidize Cu^0 to Cu^+, allowing higher surface Cu^+ species and better copper dispersion [17]. Thus, Mn^{3+} may be the main species of manganese of our optimal catalyst. It has been widely acknowledged that the deactivation of copper-based catalysts mainly results from copper aggregation and the valence transition of cupreous species. As shown in TPR results, the reduction peak of CuO shifted to a higher temperature with the increase of manganese content,

View Article Online
DOI: 10.1039/C6RA24252A

which suggested the strong interaction between cupreous species and Mn. The long lifespan of the 3Mn-Cu-SiO_2 catalyst might resulted from the strong chemical interaction between cupreous species and Mn, which could maintain its copper valence distribution and small copper crystalline size during long time stability test.

5. Conclusion

Modifying with manganese was one of an effective way to improve catalytic performance of silica-supported copper catalysts. Among all catalysts, the 3Mn-Cu-SiO_2 catalyst exhibited the best catalytic performance. The characterization analysis showed that adding an appropriate amount of manganese to Cu-SiO_2 catalysts produced a strong interaction between cupreous species and Mn, diminished the copper crystalline size, enlarged the copper surface area and enriched the surface Cu^+ species, so as to improve catalytic activity and stability of the 3Mn-Cu-SiO_2 catalyst.

References

1. J. Goldemberg, *science*, 2007, **315**, 808-810.
2. M. A. Sadiq, Y. K. Ali and A. R. Noor, *Eng. Technol. J*, 2011, **29**, 1438-1450.
3. M. Balat and H. Balat, *Appl. Energy*, 2009, **86**, 2273-2282.
4. G. J. Sunley and D. J. Watson, *Catal. Today*, 2000, **58**, 293-307.
5. M. Rosen and D. Scott, *Int. J. Hydrogen. Energ*, 1988, **13**, 617-623.
6. F. T. van de Scheur and L. H. Staal, *Appl. Catal. A Gen*, 1994, **108**, 63-83.
7. Y. Zhu, Y. Zhu, G. Ding, S. Zhu, H. Zheng and Y. Li, *Appl. Catal. A Gen*, 2013, **468**, 296-304.
8. T. Turek, D. Trimm and N. Cant, *Catal. Rev. Sci. Eng*, 1994, **36**, 645-683.
9. Z. He, H. Lin, P. He and Y. Yuan, *J. Catal*, 2011, **277**, 54-63.
10. J. Zheng, W. Zhu, C. Ma, M. Jia, Z. Wang, Y. Hou and W. Zhang, *Pol. J. Chem*, 2009, **83**, 1379-1387.
11. A. Yin, X. Guo, W.-L. Dai and K. Fan, *J. Phys. Chem. C*, 2009, **113**, 11003-11013.
12. J. Gong, H. Yue, Y. Zhao, S. Zhao, L. Zhao, J. Lv, S. Wang and X. Ma, *J. Am. Chem. Soc*, 2012, **134**, 13922-13925.

View Article Online
DOI: 10.1039/C6RA24252A

13. Y.-Y. Zhu, S.-R. Wang, L.-J. Zhu, X.-L. Ge, X.-B. Li and Z.-Y. Luo, *Catal. Lett*, 2010, **135**, 275-281.
14. S. Zhao, H. Yue, Y. Zhao, B. Wang, Y. Geng, J. Lv, S. Wang, J. Gong and X. Ma, *J. Catal*, 2013, **297**, 142-150.
15. A. Yin, J. Qu, X. Guo, W.-L. Dai and K. Fan, *Appl. Catal. A Gen*, 2011, **400**, 39-47.
16. F. T. van de Scheur, D. S. Brands, B. van der Linden, C. O. Luttikhuis, E. K. Poels and L. H. Staal, *Appl. Catal. A Gen*, 1994, **116**, 237-257.
17. H. Chen, J. Lin, K. Tan and J. Li, *Appl. Surf. Sci*, 1998, **126**, 323-331.
18. Y.-m. Zhu and X. W. L. Shi, *Bull. Kor. Chem. Soc*, 2014, **35**, 141-146.
19. J.-H. Fei, M.-X. Yang, Z.-Y. Hou and X.-M. Zheng, *Energ. Fuels*, 2004, **18**, 1584-1587.
20 S-R. Wang, W-W. Guo, H-X. Wang, L-J. Zhu and K-Z. Qiu, *Catal. Lett*, 2014, **144**, 1305-1312.
21. A. Yin, C. Wen, X. Guo, W.-L. Dai and K. Fan, *J. Catal*, 2011, **280**, 77-88.
22. J. Evans, M. Wainwright, A. Bridgewater and D. Young, *Appl. Catal*, 1983, **7**, 75-83.
23. C.-L. Ye, C.-L. Guo and J.-L. Zhang, *Fuel. Process. Technol*, 2016, **143**, 219-224.
24. A. Dandekar and M. Vannice, *J. Catal*, 1998, **178**, 621-639.
25. Y. Huang, H. Ariga, X. Zheng, X. Duan, S. Takakusagi, K. Asakura and Y. Yuan, *J. Catal*, 2013, **307**, 74-83.
26. J. Xue, X. Wang, G. Qi, J. Wang, M. Shen and W. Li, *J. Catal*, 2013, **297**, 56-64.
27. A. Bienholz, R. Blume, A. Knop-Gericke, F. Girgsdies, M. Behrens and P. Claus, *J. Phys. Chem. C*, 2010, **115**, 999-1005.
28. H.-Y. Zheng, Y.-L. Zhu, L. Huang, Z.-Y. Zeng, H.-J. Wan and Y.-W. Li, *Catal. Commun*, 2008, **9**, 342-348.
29. W. Li, M. Zhuang, T. Xiao and M. Green, *J. Phys. Chem. B*, 2006, **110**, 21568-21571.

View Article Online
DOI: 10.1039/C6RA24252A

30. K.-Y. Lee, C.-C. Shen and Y.-J. Huang, *Ind. Eng. Chem. Res*, 2014, **53**, 12622-12630.

31. J. Moulder, W. Stickle, P. Sobol, K. Bomben and J. Chastain, *Physical Electronics Division*, 1992.

32. B. Zhang, Y. Zhu, G. Ding, H. Zheng and Y. Li, *Appl. Catal. A Gen*, 2012, **443**, 191-201.

33. K. Sun, W. Lu, F. Qiu, S. Liu and X. Xu, *Appl. Catal. A Gen*, 2003, **252**, 243-249.

34. L.-F. Chen, P.-J. Guo, M.-H. Qiao, S.-R. Yan, H.-X. Li, W. Shen, H.-L. Xu and K.-N. Fan, *J. Catal*, 2008, **257**, 172-180.

35. S. Wang, X. Li, Q. Yin, L. Zhu and Z. Luo, *Catal. Commun*, 2011, **12**, 1246-1250.

36. K-Z. Qiu, W-W. Guo, H-X. Wang, L-J. Zhu and S-R. Wang, *Acta Phys. -Chim. Sin*, 2015, **31**, 1129-1136.

37. H. F. Franzen, M. X. Umaña, J. McCreary and R. Thorn, *J. Solid State Chem*, 1976, **18**, 363-368.

Figure captions

Fig. 1. Catalytic performance of the catalysts as a function of reaction time. Reaction condition: T=523 K, P=3.0 MPa, H_2/MA=15 (mol/mol), LHSV=2 h^{-1}.

Fig. 2. XRD patterns of the calcined (A) and reduced (B) catalysts with different Mn contents.

Fig. 3. H_2-TPR patterns of the catalysts with different manganese contents.

Fig. 4. Mn 2P XPS spectra of the reduced catalysts

Fig. 5. Cu 2P XPS spectra of the reduced catalysts with different manganese contents.

Fig. 6. XAES spectra of the reduced catalysts with different manganese contents.

View Article Online
DOI: 10.1039/C6RA24252A

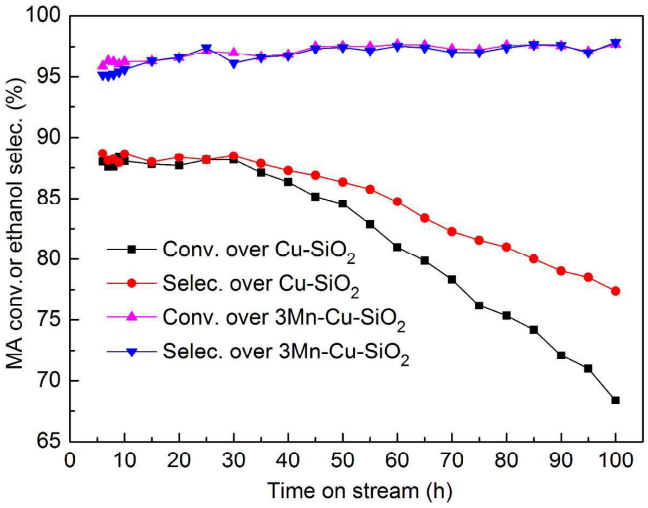

Fig. 1. Catalytic performance of the catalysts as a function of reaction time. Reaction condition: T=523 K, P=3.0 MPa, H_2/MA=15 (mol/mol), LHSV=2 h^{-1}.

View Article Online
DOI: 10.1039/C6RA24252A

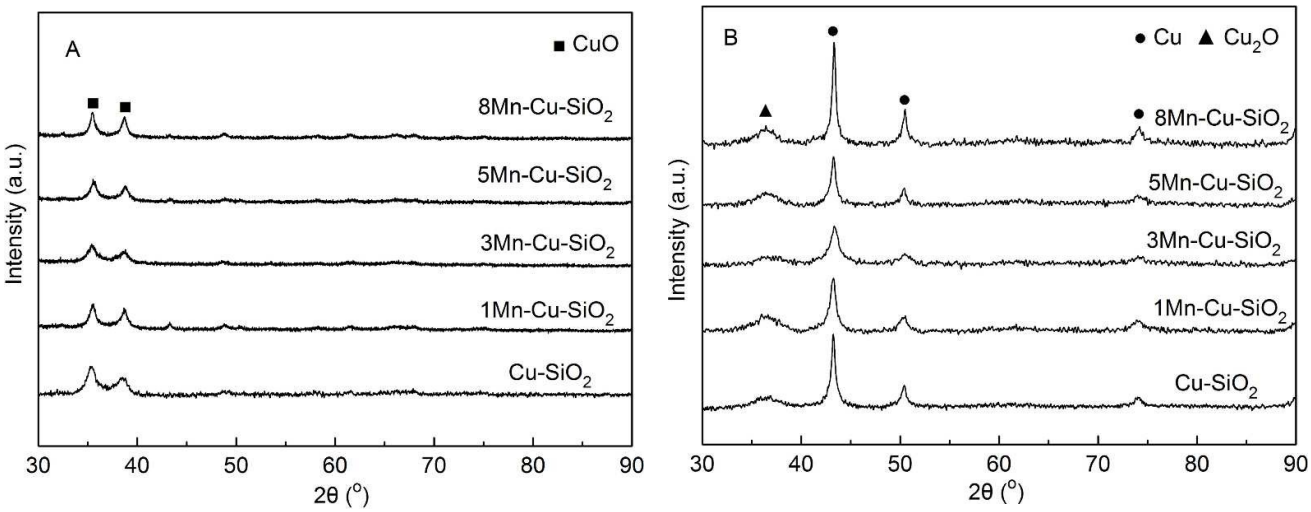

Fig. 2. XRD patterns of the calcined (A) and reduced (B) catalysts with different Mn.

View Article Online
DOI: 10.1039/C6RA24252A

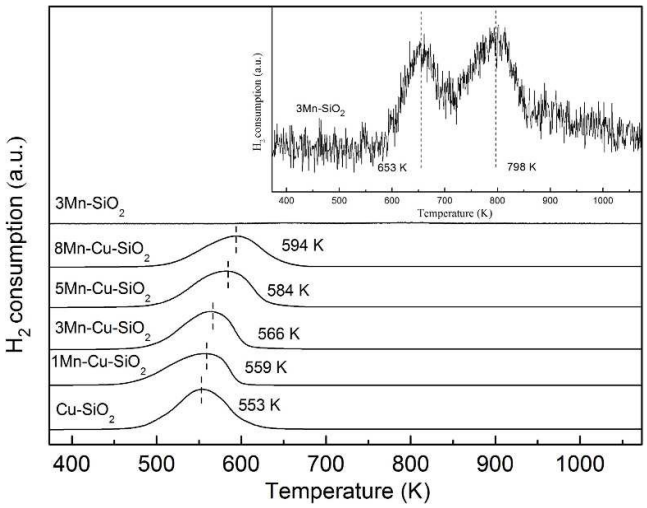

Fig. 3. H_2-TPR patterns of the catalysts with different manganese contents.

View Article Online
DOI: 10.1039/C6RA24252A

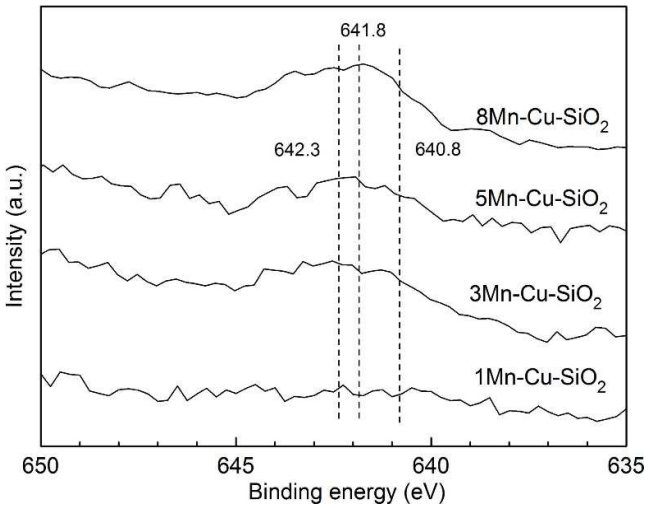

Fig. 4. Mn 2P XPS spectra of the reduced catalysts.

View Article Online
DOI: 10.1039/C6RA24252A

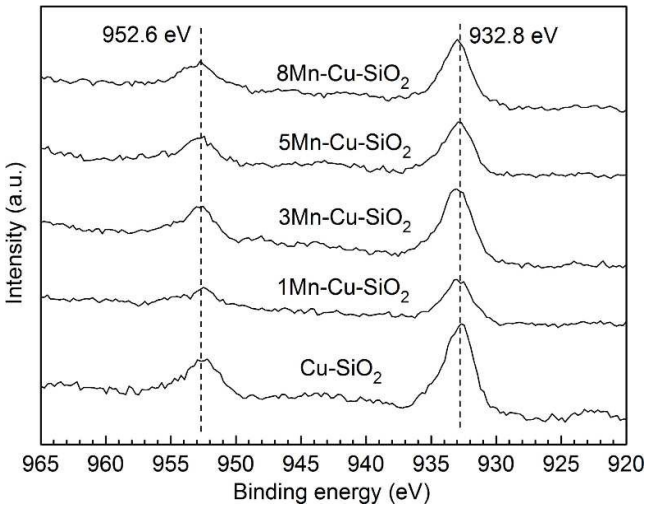

Fig. 5. Cu 2P XPS spectra of the reduced catalysts with different manganese contents.

View Article Online
DOI: 10.1039/C6RA24252A

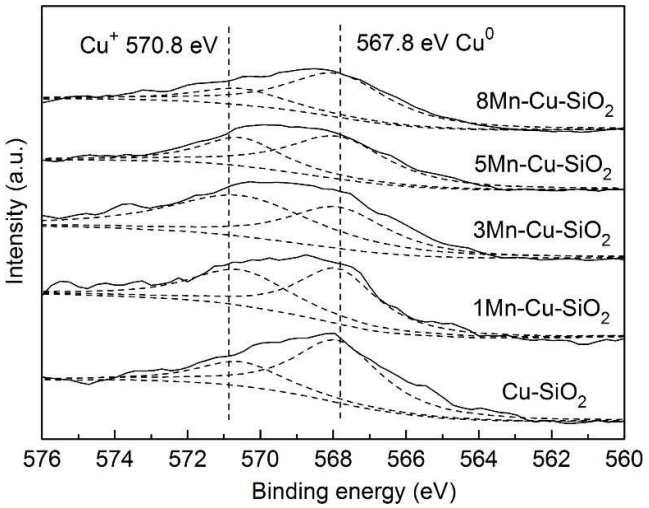

Fig. 6. XAES spectra of the reduced catalysts with different manganese contents.

View Article Online
DOI: 10.1039/C6RA24252A

Table 1
Activity of the catalysts with different manganese content

Catalyst	Conversion of MA (%)	Selectivity of Ethanol (%)	Yield of Ethanol (%)
Cu-SiO_2	87.6	88.2	77.3
1Mn-Cu-SiO_2	92.0	91.2	83.9
3Mn-Cu-SiO_2	96.2	95.2	91.6
5Mn-Cu-SiO_2	90.1	89.1	80.3
8Mn-Cu-SiO_2	42.7	65.1	27.8
3Mn-SiO_2	0	-	-

Reaction condition: T=523 K, P=3.0 MPa, H_2/MA=15 (mol/mol), LHSV=2 h^{-1}.

View Article Online
DOI: 10.1039/C6RA24252A

Table 2

Physicochemical properties of xMn-Cu-SiO_2 catalysts with different Mn contents

Catalyst	BET surface area (m^2/g)	Pore volume (m^3/g)	Average pore size (nm)	d_{Cu} (nm)[a]	X_{Cu+} (%)[b]	Cu surface area[c] (m^2/g)
Cu-SiO_2	316	0.54	6.9	19.2	27.9	20.3
1Mn-Cu-SiO_2	288	0.54	7.5	14.1	44.8	26.0
3Mn-Cu-SiO_2	260	0.63	9.7	12.5	58.5	30.9
5Mn-Cu-SiO_2	133	0.39	11.8	15.7	34.5	25.1
8Mn-Cu-SiO_2	59	0.22	14.6	22.6	24.8	15.4

[a] Obtained by the Scherrer equation from the XRD data.

[b] Mole ratio of $Cu^+/(Cu^0+Cu^+)$ determined by Cu LMM XAES spectra.

[b] Determined by N_2O chemisorption.